# Optimized SESAMs for kilowatt-level ultrafast lasers

**A. Diebold,[1,*] T. Zengerle,[1] C. G. E. Alfieri,[1] C. Schriber,[1] F. Emaury,[1] M. Mangold,[1] M. Hoffmann,[2] C. J. Saraceno,[1] M. Golling,[1] D. Follman,[3] G. D. Cole,[3,4] M. Aspelmeyer,[5] T. Südmeyer,[2] and U. Keller[1]**

[1]*Institute for Quantum Electronics, ETH Zurich, Auguste-Piccard-Hof 1, 8093 Zurich, Switzerland*
[2]*Laboratoire Temps-Fréquence, Université de Neuchâtel, 2000 Neuchâtel, Switzerland*
[3]*Crystalline Mirror Solutions LLC, 114 E Haley, Suite G, Santa Barbara, California 93101, USA*
[4]*Crystalline Mirror Solutions GmbH, Parkring 10, A-1010 Vienna, Austria*
[5]*Vienna Center for Quantum Science and Technology (VCQ), Faculty of Physics, University of Vienna, A-1090 Vienna, Austria*
**diebold@phys.ethz.ch*

**Abstract:** We present a thorough investigation of surface deformation and thermal properties of high-damage threshold large-area semiconductor saturable absorber mirrors (SESAMs) designed for kilowatt average power laser oscillators. We compare temperature rise, thermal lensing, and surface deformation of standard SESAM samples and substrate-removed SESAMs contacted using different techniques. We demonstrate that for all cases the thermal effects scale linearly with the absorbed power, but the contacting technique critically affects the strength of the temperature rise and the thermal lens of the SESAMs (i.e. the slope of the linear change). Our best SESAMs are fabricated using a novel substrate-transfer direct bonding technique and show excellent surface flatness (with non-measureable radii of curvature (ROC), compared to astigmatic ROCs of up to 10 m for standard SESAMs), order-of-magnitude improved heat removal, and negligible deformation with absorbed power. This is achieved without altering the saturation behavior or the recovery parameters of the samples. These SESAMs will be a key enabling component for the next generation of kilowatt-level ultrafast oscillators.

©2016 Optical Society of America

**OCIS codes:** (140.0140) Lasers and laser optics; (140.7090) Ultrafast lasers; (140.4050) Mode-locked lasers.

## References and links

1. U. Keller, "Recent developments in compact ultrafast lasers," Nature **424**(6950), 831–838 (2003).
2. T. Südmeyer, S. V. Marchese, S. Hashimoto, C. R. E. Baer, G. Gingras, B. Witzel, and U. Keller, "Femtosecond laser oscillators for high-field science," Nat. Photonics **2**(10), 599–604 (2008).
3. T. Eidam, S. Hanf, E. Seise, T. V. Andersen, T. Gabler, C. Wirth, T. Schreiber, J. Limpert, and A. Tünnermann, "Femtosecond fiber CPA system emitting 830 W average output power," Opt. Lett. **35**(2), 94–96 (2010).
4. P. Russbueldt, T. Mans, J. Weitenberg, H. D. Hoffmann, and R. Poprawe, "Compact diode-pumped 1.1 kW Yb:YAG Innoslab femtosecond amplifier," Opt. Lett. **35**(24), 4169–4171 (2010).
5. A. Giesen, H. Hügel, A. Voss, K. Wittig, U. Brauch, and H. Opower, "Scalable concept for diode-pumped high-power solid-state lasers," Appl. Phys. B **58**(5), 365–372 (1994).
6. C. J. Saraceno, F. Emaury, O. H. Heckl, C. R. E. Baer, M. Hoffmann, C. Schriber, M. Golling, T. Südmeyer, and U. Keller, "275 W average output power from a femtosecond thin disk oscillator operated in a vacuum environment," Opt. Express **20**(21), 23535–23541 (2012).
7. C. J. Saraceno, F. Emaury, C. Schriber, M. Hoffmann, M. Golling, T. Südmeyer, and U. Keller, "Ultrafast thin-disk laser with 80 μJ pulse energy and 242 W of average power," Opt. Lett. **39**(1), 9–12 (2014).
8. C. J. Saraceno, F. Emaury, C. Schriber, A. Diebold, M. Hoffmann, M. Golling, T. Suedmeyer, and U. Keller, "Toward millijoule-level high-power ultrafast thin-disk oscillators," IEEE J. Sel. Top. Quantum Electron. **1**(1), (2015).
9. F. Emaury, A. Diebold, A. Klenner, C. J. Saraceno, S. Schilt, T. Südmeyer, and U. Keller, "Frequency comb offset dynamics of SESAM modelocked thin disk lasers," Opt. Express **23**(17), 21836–21856 (2015).

#260443 Received 3 Mar 2016; revised 13 Apr 2016; accepted 13 Apr 2016; published 4 May 2016
© 2016 OSA

10. J. Brons, V. Pervak, E. Fedulova, D. Bauer, D. Sutter, V. Kalashnikov, A. Apolonskiy, O. Pronin, and F. Krausz, "Energy scaling of Kerr-lens mode-locked thin-disk oscillators," Opt. Lett. **39**(22), 6442–6445 (2014).
11. U. Keller, D. A. B. Miller, G. D. Boyd, T. H. Chiu, J. F. Ferguson, and M. T. Asom, "Solid-state low-loss intracavity saturable absorber for Nd:YLF lasers: an antiresonant semiconductor Fabry-Perot saturable absorber," Opt. Lett. **17**(7), 505–507 (1992).
12. U. Keller, K. J. Weingarten, F. X. Kärtner, D. Kopf, B. Braun, I. D. Jung, R. Fluck, C. Hönninger, N. Matuschek, and J. Aus der Au, "Semiconductor saturable absorber mirrors (SESAMs) for femtosecond to nanosecond pulse generation in solid-state lasers," IEEE J. Sel. Top. Quantum Electron. **2**(3), 435–453 (1996).
13. F. X. Kärtner and U. Keller, "Stabilization of solitonlike pulses with a slow saturable absorber," Opt. Lett. **20**(1), 16–18 (1995).
14. R. Paschotta and U. Keller, "Passive mode locking with slow saturable absorbers," Appl. Phys. B **73**(7), 653–662 (2001).
15. O. Pronin, J. Brons, C. Grasse, V. Pervak, G. Boehm, M. C. Amann, V. L. Kalashnikov, A. Apolonski, and F. Krausz, "High-power 200 fs Kerr-lens mode-locked Yb:YAG thin-disk oscillator," Opt. Lett. **36**(24), 4746–4748 (2011).
16. J. Aus der Au, G. J. Spühler, T. Südmeyer, R. Paschotta, R. Hövel, M. Moser, S. Erhard, M. Karszewski, A. Giesen, and U. Keller, "16.2-W average power from a diode-pumped femtosecond Yb:YAG thin disk laser," Opt. Lett. **25**(11), 859–861 (2000).
17. C. Hönninger, R. Paschotta, F. Morier-Genoud, M. Moser, and U. Keller, "Q-switching stability limits of continuous-wave passive mode locking," J. Opt. Soc. Am. B **16**(1), 46–56 (1999).
18. J. A. Au, D. Kopf, F. Morier-Genoud, M. Moser, and U. Keller, "60-fs pulses from a diode-pumped Nd:glass laser," Opt. Lett. **22**(5), 307–309 (1997).
19. U. Keller, "Ultrafast solid-state lasers," in *Landolt-Börnstein. Laser Physics and Applications, Subvolume B: Laser Systems. Part I.* G. Herziger, H. Weber, and R. Proprawe, eds. (Springer Verlag, 2007), pp. 33–167.
20. C. J. Saraceno, C. Schriber, M. Mangold, M. Hoffmann, O. H. Heckl, C. R. E. Baer, M. Golling, T. Südmeyer, and U. Keller, "SESAMs for high-power oscillators: design guidelines and damage thresholds," IEEE J. Sel. Top. Quantum Electron. **18**(1), 29–41 (2012).
21. C. J. Saraceno, C. Schriber, F. Emaury, O. H. Heckl, C. R. E. Baer, M. Hoffmann, K. Beil, C. Kränkel, M. Golling, T. Südmeyer, and U. Keller, "Cutting-edge high-power ultrafast thin disk oscillators," Appl. Sci. **3**(2), 355–395 (2013).
22. T. Südmeyer, C. Kränkel, C. R. E. Baer, O. H. Heckl, C. J. Saraceno, M. Golling, R. Peters, K. Petermann, G. Huber, and U. Keller, "High-power ultrafast thin disk laser oscillators and their potential for sub-100-femtosecond pulse generation," Appl. Phys. B **97**(2), 281–295 (2009).
23. V. Magni, "Multielement stable resonators containing a variable lens," J. Opt. Soc. Am. A **4**(10), 1962–1969 (1987).
24. C. R. E. Baer, O. H. Heckl, C. J. Saraceno, C. Schriber, C. Kränkel, T. Südmeyer, and U. Keller, "Frontiers in passively mode-locked high-power thin disk laser oscillators," Opt. Express **20**(7), 7054–7065 (2012).
25. G. D. Cole, W. Zhang, M. J. Martin, J. Ye, and M. Aspelmeyer, "Tenfold reduction of Brownian noise in optical interferometry," Nat. Photonics **7**(8), 644–650 (2013).
26. M. Haiml, U. Siegner, F. Morier-Genoud, U. Keller, M. Luysberg, R. C. Lutz, P. Specht, and E. R. Weber, "Optical nonlinearity in low-temperature-grown GaAs: Microscopic limitations and optimization strategies," Appl. Phys. Lett. **74**(21), 3134–3136 (1999).
27. C. J. Saraceno, O. H. Heckl, C. R. E. Baer, C. Schriber, M. Golling, K. Beil, C. Kränkel, T. Südmeyer, G. Huber, and U. Keller, "Sub-100 femtosecond pulses from a SESAM modelocked thin disk laser," Appl. Phys. B **106**(3), 559–562 (2012).
28. A. Diebold, F. Emaury, C. J. Saraceno, C. Schriber, M. Golling, T. Suedmeyer, and U. Keller, "62-fs pulses from a SESAM modelocked Yb:CALGO thin disk laser," Opt. Lett. **38**(19), 3842–3845 (2013).
29. U. Keller and A. C. Tropper, "Passively modelocked surface-emitting semiconductor lasers," Phys. Rep. **429**(2), 67–120 (2006).
30. R. Häring, R. Paschotta, A. Aschwanden, E. Gini, F. Morier-Genoud, and U. Keller, "High–power passively mode–locked semiconductor lasers," IEEE J. Quantum Electron. **38**(9), 1268–1275 (2002).
31. D. J. H. C. Maas, B. Rudin, A.-R. Bellancourt, D. Iwaniuk, S. V. Marchese, T. Südmeyer, and U. Keller, "High precision optical characterization of semiconductor saturable absorber mirrors," Opt. Express **16**(10), 7571–7579 (2008).
32. M. Haiml, R. Grange, and U. Keller, "Optical characterization of semiconductor saturable absorbers," Appl. Phys. B **79**(3), 331–339 (2004).
33. S. L. Schieffer, J. A. Berger, B. L. Rickman, V. P. Nayyar, and W. A. Schroeder, "Thermal effects in semiconductor saturable-absorber mirros," J. Opt. Soc. Am. B **29**(4), 543–552 (2012).
34. C. Schriber, F. Emaury, A. Diebold, S. Link, M. Golling, K. Beil, C. Kränkel, C. J. Saraceno, T. Südmeyer, and U. Keller, "Dual-gain SESAM modelocked thin disk laser based on Yb:$Lu_2O_3$ and Yb:$Sc_2O_3$," Opt. Express **22**(16), 18979–18986 (2014).
35. W. Winkler, K. Danzmann, A. Rüdiger, and R. Schilling, "Heating by optical absorption and the performance of interferometric gravitational-wave detectors," Phys. Rev. A **44**(11), 7022–7036 (1991).

#260443 Received 3 Mar 2016; revised 13 Apr 2016; accepted 13 Apr 2016; published 4 May 2016
© 2016 OSA

## 1. Introduction

Many disciplines in science and technology require ultrafast laser sources with ever-increasing average and peak power at megahertz repetition rates [1, 2]. Examples include laser precision micromachining, frequency metrology from the infrared to the extreme ultraviolet, and strong field laser physics in attosecond science. In the last decade, spectacular progress has been achieved with Yb-doped laser sources in various geometries. Ultrafast laser systems based on amplifiers nowadays can operate beyond the kilowatt average power regime [3, 4], whereas ultrafast oscillators employing the thin disk geometry [5–7] already alone reach comparable average power levels of several hundreds of watts. These modelocked thin disk lasers (TDLs) reach the targeted parameter range with a single laser oscillator cavity, reliable passive modelocking, and low noise performance [8, 9]. Such lasers currently reach the highest average power (275 W [6, 10]) and highest pulse energy (80 µJ [7]) of any ultrafast laser oscillator technology. So far, most modelocked TDLs that were demonstrated used semiconductor saturable absorber mirrors (SESAMs) [11, 12] for starting and stabilizing the soliton modelocking [13, 14], although significant progress was also obtained using Kerr-lens modelocking [10, 15].

We continue to focus our efforts on the development of high power SESAM-modelocked TDLs [8, 16]. SESAMs are ideally suited for power scaling of ultrafast thin disk oscillators as their micrometer thin structures, in combination with large (up to a few millimeters in diameters) laser spot sizes facilitate a quasi-1D heat flow, similar to the thin disk gain medium. In this regime, the output power of the modelocked oscillator can be increased by simply enlarging the area of the laser spot on the absorber and on the gain medium accordingly. In contrast to Kerr-lens modelocking, SESAMs provide reliable self-starting modelocking and additionally allow for the oscillator to be modelocked in the middle of its cavity stability zone with a full decoupling of spatial and temporal effects. This becomes even more important for the targeted high average power and high pulse energy. In addition, SESAMs offer a high level of flexibility. By adjusting their multi-layer design important modelocking parameters such as saturation fluence, roll-over coefficient, and modulation depth can be adapted to a given type of laser geometry. This helps to achieve optimized and reliable continuous wave (cw) modelocking of a large variety of laser systems without instabilities such as Q-switched modelocking (QML) [17] or multiple pulsing [18, 19]. Furthermore, we recently presented design guidelines to increase the damage threshold for SESAMs specifically designed for high power oscillators [20]. We identified the main damage mechanism as two-photon-absorption (TPA) which can be minimized with appropriate material and multi-layer designs. The optimized design guidelines enabled the scaling of the average output power to 275 W [6] and of the output pulse energy to 80 µJ [7]. These SESAMs were designed for operation in high power modelocked TDLs and have very low nonsaturable losses (typically <0.1%), which have so far minimized unwanted thermal effects. In addition, in modelocked operation the SESAM is typically fully saturated to minimize any additional saturable loss.

However, as modelocked TDLs approach the kilowatt average output power regime, the remaining extremely small nonsaturable SESAM loss can nevertheless become problematic and result in a significant temperature rise and thermal deformation. For a better understanding, we can quantify these effects for a future kilowatt-class TDL cavity, see Fig. 1. In simple oscillator geometries, i.e. with a small number of gain passes, output coupling coefficients in the range of 10% will be used. This leads to intracavity powers exceeding 10 kW. Using a low-loss SESAM with 0.1% nonsaturable loss then results in >10 W of deposited heat, which can cause significant thermal effects if spot sizes are not increased accordingly. Furthermore, there is a strong interest in high power modelocking with shorter pulses (<100 fs) [21, 22] which typically requires SESAMs with faster absorber recovery dynamics and higher modulation depths at the expense of a larger nonsaturable

#260443 Received 3 Mar 2016; revised 13 Apr 2016; accepted 13 Apr 2016; published 4 May 2016
© 2016 OSA

loss [13, 14]. Thus the above mentioned thermal effects will become even more pronounced. The thermal SESAM lensing can be reduced with a larger laser beam mode size on the SESAM which means that the mode diameter has to be increased from typically a few millimeters to a few centimeters. This however makes cavity designs increasingly sensitive to even very small surface deformations, arising both from aberrations of the "cold" surface (i.e. without any absorbed power) and from thermal lensing, see Fig. 1 and [23, 24]. In our most recent results [6, 7], laser spot sizes on the absorber >1.2 mm radius could not be used without compromising the beam quality and modelocking stability. Therefore, improving the surface quality and thermal deformation of high power SESAMs is a crucial step for further output scaling.

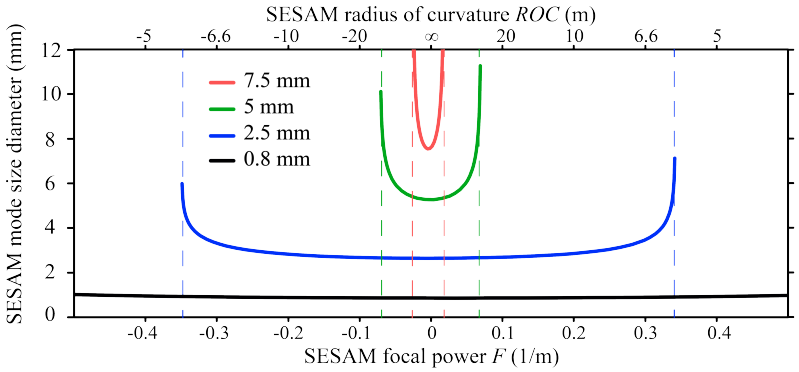


Fig. 1. Simulation of laser cavity stability zones for different SESAM mode size diameters ranging from 0.8 mm, 2.5 mm, 5 mm to 7.5 mm, optimized for initially perfectly flat SESAMs. The cavity design for 2.5 mm SESAM laser spot diameter (blue) is similar to what is used in our current high power thin disk laser cavities, such as in the 275 W average power result [6]. A beam diameter of 5 mm (green) and 7.5 mm (red) with constant SESAM fluences would allow for intracavity average powers of approximately 4 times and 9 times the current values, respectively. In general, the width of the stability zone decreases approximately inversely proportional to the square of the SESAM mode size. In order for the cavity to remain stable, the SESAM focal power $F$ (related for radially symmetric samples to the radius of curvature $ROC$ via $F = 2/ROC$) must not change by more than approximately 0.35 $m^{-1}$ compared to its cold value (2.5 mm of initial mode size), 0.07 $m^{-1}$ (5 mm of initial mode size), and roughly 0.03 $m^{-1}$ (7.5 mm of initial mode size). Thus, for larger mode sizes we even need to improve the flatness of the cold SESAMs (i.e. without any absorbed power) in order to ensure that astigmatisms are minimized. Additionally, SESAM thermal lensing needs to be addressed. We experimentally observed that increasing the beam diameter beyond 2.5 mm on non-optimized standard SESAMs leads to cavity instabilities.

Here, we address this challenge and present a thorough study of the surface aberrations and thermal properties of various SESAMs designed for high power oscillators. To the best of our knowledge, we carry out for the first time systematic measurements of the cold surface flatness, temperature rise as a function of absorbed laser power, and thermal lensing effects of different SESAMs. In this goal, we study three types of SESAMs that are bonded to various heat sinks using different bonding and substrate-removal techniques, see Fig. 2, showing that:

- the absorber parameters remain unchanged for all post-processing and bonding techniques,
- the initial cold surface deformation is strongly influenced by the contacting method and requires our presented optimized techniques for future laser spot size scaling,
- the increase in temperature and focal power (focal power $F = 2/(\mathrm{ROC})$, with the radius of curvature ROC) under continuous wave or pulsed operation shows a linear

#260443 Received 3 Mar 2016; revised 13 Apr 2016; accepted 13 Apr 2016; published 4 May 2016
© 2016 OSA

dependence with the average power absorbed by the SESAM, with the proportionality factor depending on the contacting technique.

As a result of our investigation, SESAMs on SiC heat sinks with improved heat removal, stiffness, and cold surface flatness were developed which will be a key enabling element for future average power and pulse energy scaling of modelocked oscillators. In the following sections of the paper we will present in more detail the SESAM designs, bonding and measurement techniques, and the cold and absorption-induced SESAM lensing under continuous wave and pulsed operation. They can serve as reference for future absorber development using also other optimized heat sink materials.

## 2. SESAM samples used for the study

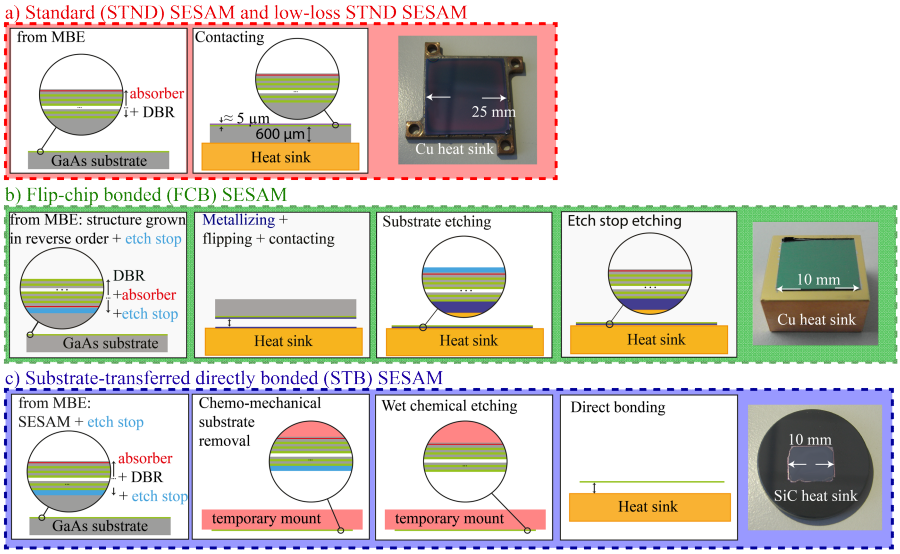


Fig. 2. Schematics of the different bonding techniques presented in this paper. Color code: gray – GaAs, green – AlAs, red – quantum well absorber section, light blue – etch stop, dark blue - metallization. a) For STND SESAMs, the molecular beam epitaxy grown structure and GaAs substrate are solder-bonded onto the heat sink, usually made of copper. b) For FCB SESAMs, the upside-down grown structure (including an etch stop layer between absorber and GaAs substrate) is metallized and vacuum soldered to a polished copper heat sink. Subsequently, the substrate and the etch stop layer are removed by wet etching. c) For the STB SESAMs contacted by Crystalline Mirror Solutions [25], an etch stop layer is grown between the GaAs substrate and the distributed Bragg reflector section. After growth, the GaAs substrate is removed by a chemo-mechanical etching process, which is followed by a selective wet chemical etch stop removal step. Finally, the remaining layers are directly bonded onto the heat sink, in this case polished silicon carbide. The far right picture for each bonding technique contains a photograph of the finalized samples.

### *2.1 Epitaxial structure*

For our study, we grew SESAM structures by molecular beam epitaxy (MBE) in the FIRST cleanroom facility at ETH Zurich. The design of our structures follows closely the guidelines presented in [20] for high-damage threshold samples. Our absorber section consists of three 10-nm thick InGaAs quantum well (QW) absorber layers surrounded by AlAs barriers, placed in one antinode of the standing wave pattern of the electric field. It was grown at low temperature (280°C) in order to reach relatively short recovery times [26] in the few-ps regime. Even though in the soliton modelocking regime the recovery dynamics of the SESAM only play a minor role for the final pulse duration [13, 14], faster recovery times still

#260443 Received 3 Mar 2016; revised 13 Apr 2016; accepted 13 Apr 2016; published 4 May 2016
© 2016 OSA

support even shorter pulse durations [27, 28]. Therefore, we designed our SESAMs with fast recovery dynamics to support both short pulse durations in combination with high average power. The trade-off is a slightly increased nonsaturable loss compared to slower SESAMs. The absorber section was grown on a 30-pair GaAs/AlAs distributed Bragg reflector (DBR) grown with standard temperatures (580°C) providing a high reflectivity of >99.95% at a center wavelength of 1030 nm. We use a GaAs wafer with a thickness of about 625 µm as a substrate. Between the GaAs wafer and the DBR, we additionally grew a 300-nm thick etch stop layer, required for eventual post-processing. For an enhanced damage threshold and appropriate parameters for thin disk lasers, a 2-pair quarter-wave dielectric top-coating ($SiO_x/SiN_x$) was deposited using plasma-enhanced chemical vapor deposition (PECVD) on all samples.

In order to investigate the influence of the nonsaturable losses on the thermal properties of our SESAMs (i.e. temperature and focal power increase under optical load), we also included in our study a second similar SESAM structure but with the absorber section grown at a slightly higher temperature of 300°C and a 3-pair quarter-wave dielectric top-coating. This results in slower recovery times, but also in a higher damage threshold and lower nonsaturable loss which was used for our record modelocking performance in our previous experiments [6, 7]. For this second SESAM we did not remove the GaAs wafer and therefore refer to as the "low-loss standard SESAM".

*2.2 Contacting techniques*

The mounting or contacting techniques can be summarized as follows in more detail (according to Fig. 2):

a) Standard (STND) SESAMs, see Fig. 2(a): These SESAMs were mounted by soldering a 1x1 $cm^2$ part of the structure (including the GaAs substrate) directly onto a Cu substrate. The solder consisted of 45% Pb and 55% Bi.

b) Flip-chip bonded (FCB) SESAMs, see Fig. 2(b): For these SESAMs, the above presented structure was grown in an upside-down fashion, i.e. with the absorber layer grown before the DBR and an additional etch stop layer between the GaAs substrate and absorber section. Both the polished Cu heat sinks (<4 Å rms surface roughness) and the GaAs-based sample (1x1 $cm^2$) were metallized (30 nm of Ti, 20 nm of Pt, 100 nm of Au, and 30 nm of Ti, 20 nm of Pt, 5000 nm of In, 100 nm of Au). Next, these pieces were soldered under vacuum conditions (<$5x10^{-5}$ mbar), where, at the junction, a uniform pressure of ≈3 bar was applied at a temperature of ≈200°C. After soldering, the GaAs substrate and the etch stop layer were removed with wet chemical etching using citric acid and dilute hydrogen fluoride, respectively. This substrate-removal procedure is common practice for semiconductor disk lasers [29, 30].

c) Substrate-transferred directly bonded (STB) SESAMs supplied by Crystalline Mirror Solutions, see Fig. 2(c): A similarly sized chip of the same epitaxial material as used for our STND SESAMs was processed by Crystalline Mirror Solutions [25]. Here, the sample was first attached to a temporary mount and the GaAs substrate was removed via a chemo-mechanical process, followed by selective wet chemical etching to eliminate the etch stop layer. Next, the epitaxial material was directly bonded to a polished (≈1 Å rms surface roughness) SiC substrate and the temporary mounting material was cleaned from the sample surface. The SiC substrates have an excellent combination of high thermal conductivity (≈300 $Wm^{-1}K^{-1}$) and high stiffness (Young's modulus of 460 GPa). This value is comparable to Cu (thermal conductivity of ≈400 $Wm^{-1}K^{-1}$) but with a much higher Young's modulus (120 GPa for Cu).

#260443 Received 3 Mar 2016; revised 13 Apr 2016; accepted 13 Apr 2016; published 4 May 2016
© 2016 OSA

*2.3 Nonlinear reflectivity and recovery dynamics of the samples*

In order to investigate the influence of the contacting methods on the SESAM parameters, we measured nonlinear reflectivity and recovery dynamics of our mounted samples. All measurements are presented in Fig. 3. For the nonlinear reflectivity measurements we used a high precision nonlinear reflectivity characterization setup [31] and a SESAM-modelocked thin disk laser delivering 6 W of average power at a center wavelength of 1030 nm, a pulse duration of 1 ps, and a pulse repetition rate of 3.9 MHz, resulting in a pulse energy of 1.5 µJ, similar to what was used in [20]. The recovery dynamics were measured using a standard pump-probe setup with a laser delivering up to 800 mW of average output power with pulse durations of 300 fs, a center wavelength of 1030 nm, and a pulse repetition rate of 80 MHz (i.e. pulse energies up to 10 nJ).

All samples (STND, FCB, STB) were measured after the dielectric topcoating mentioned in the previous paragraph had been applied and exhibit nearly the same modulation depth (≈1.3%) and saturation fluence (≈80 µJ/cm$^2$). The nonsaturable losses of the FCB SESAM (0.4%) were slightly lower than the ones of the STND and STB SESAM (0.5%), see Fig. 3(b), due to absorber annealing during the upside-down growth. This also resulted in a slower 1/e recovery time of the FCB sample (1.9 ps) compared to STND and STB SESAMs (1.2 ps), see Fig. 3(a). While the surfaces of STND and FCB SESAMs showed no defects, small surface imperfections were observed after processing in the case of the samples directly bonded on SiC (STB samples), which did not affect the loss level of the samples for small spot sizes. These imperfections arise from the epitaxial growth and are currently in the process of being optimized.

The values measured for all samples are ideal for SESAMs used in high power ultrafast oscillators and confirm that post-processing and contacting has negligible effects on the SESAM parameters. In addition, the fast recovery times of these SESAMs are beneficial for sub-100-fs pulse durations [28] and are achieved with low nonsaturable losses (<0.5%). For applications targeting longer (several hundred femtoseconds) pulse durations, the absorber section can be fabricated at higher temperature [6], resulting in almost vanishing nonsaturable losses [26]. To quantify the effect of these nonsaturable losses on SESAM thermal performance, we included into our study an additional sample optimized for lowest nonsaturable losses, i.e. the "low-loss STND" sample presented in Section 2.1. This SESAM has similar parameters as the SESAMs presented here (a modulation depth of 1.1%, and a saturation fluence of 120 µJ/cm$^2$) but vanishing nonsaturable losses <0.1%, at the expense of a somewhat longer 1/e recovery time of 50 ps, see Fig. 3.

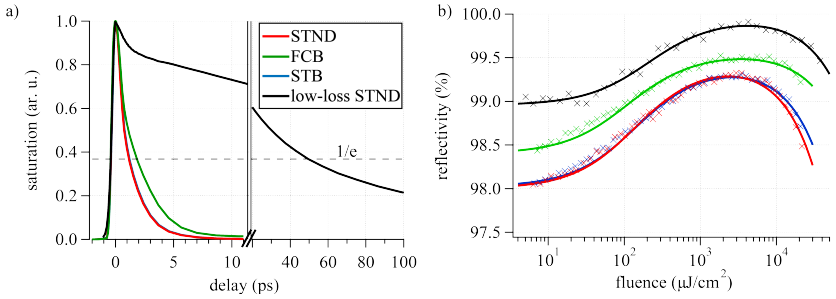


Fig. 3. Measurements of recovery dynamics and nonlinear reflectivity of different SESAMs used for this study: a) Pump-probe measurements with $t_{1/e,\,STND}$ = 1.0 ps (red), $t_{1/e,FCB}$ = 1.9 ps (green), $t_{1/e,STB}$ = 1.2 ps (blue), $t_{1/e,low\text{-}lossSTND}$ = 50 ps (black). b) Nonlinear reflectivity measurements; the solid lines represent least-squared fits. Resulting parameters (according to [32]): STND SESAM: $F_{sat}$ = 81 µJ/cm$^2$, $\Delta R$ = 1.4%, $\Delta R_{ns}$ = 0.5%, $F_2$ = 2430 mJ/cm$^2$, FCB SESAM: $F_{sat}$ = 63 µJ/cm$^2$, $\Delta R$ = 1.2%, $\Delta R_{ns}$ = 0.4%, $F_2$ = 7370 mJ/cm$^2$, STB SESAM: $F_{sat}$ = 81 µJ/cm$^2$, $\Delta R$ = 1.4%, $\Delta R_{ns}$ = 0.5%, $F_2$ = 4130 mJ/cm$^2$, low-loss STND SESAM: $F_{sat}$ = 120 µJ/cm$^2$, $\Delta R$ = 1.1%, $\Delta R_{ns}$ < 0.1%, $F_2$ = 7500 mJ/cm$^2$.

#260443 Received 3 Mar 2016; revised 13 Apr 2016; accepted 13 Apr 2016; published 4 May 2016
© 2016 OSA

## 3. Cold surface characterization: influence of contacting

We measured the surface quality of the different cold SESAM structures with a high precision interferometer (Trioptics µPhase PLANO S DOWN) directly after contacting, see Fig. 4. These measurements show that (see Fig. 2 for the sample definition):

- The STND and the low-loss STND SESAM soldered on Cu showed astigmatic surfaces, with typical ROCs of 19 m and −15 m in orthogonal directions. This strong deformation arises from surface deformations intrinsic to the thick GaAs wafer, bowing introduced during the growth of the strained DBR and absorber sections, and from the standard soldering technique. For example, the different coefficients of thermal expansion of GaAs (5.7 ppm/K) and Cu (16 ppm/K) lead to significant thermal stress during soldering of the sample onto the heat sink.
- The substrate-removed FCB sample shows similar surface astigmatism with ROCs of 24 m and −16 m in orthogonal directions. This is also partly caused by the soft Cu heat sink and mismatch of the coefficient of thermal expansion of sample and mount. Additionally, non-homogeneous pressures during the vacuum soldering process also affect the cold sample flatness.
- In contrast, the STB SESAM shows a nearly perfectly flat surface (except for some defect lines) within the accuracy of our interferometer (>50 m of ROC for spot sizes in the mm-range). This is because in the bonding process of STB samples no buffering layers of solder or glue are used, which results in a nearly perfectly stress-free bond.

From our measurements, see Fig. 4, it is clearly visible that due to their astigmatisms our STND and FCB SESAMs cannot be used for further scaling towards larger spot sizes (i.e. with SESAM laser beam diameters greater than 2.5 mm). Adjusting the cavity design such that the modes in the two orthogonal directions are both stable and give rise to similar mode sizes becomes increasingly challenging using the presented STND and FCB SESAMs, see Fig. 1. Spot size scaling can only be achieved with our STB SESAMs, which provide an almost perfectly flat surface without any astigmatism. In addition, the STB technique can be implemented on curved substrates down to a 10-cm ROC, which opens up further design possibilities for high power thin disk lasers and other types of laser resonators.

Nevertheless, it should be noted that significant improvement in terms of cold surface flatness is expected for future optimized STND and FCB samples by further investigating heat sink materials and improving the contacting techniques. In particular, DC60 copper diamond is a promising substrate candidate as its coefficient of thermal expansion (6.0 ppm/K) is almost matched with GaAs and it has an exceptionally high Young's modulus (410 GPa). This type of heat sink is currently being investigated.

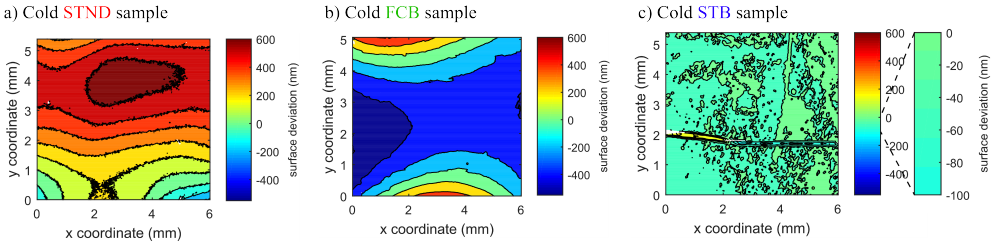


Fig. 4. Interferometric measurements of the cold surfaces of the processed SESAMs. Resulting radii of curvature (ROC): a) STND SESAM $ROC_x$ = 19 m, $ROC_y$ = −15 m; b) FCB SESAM $ROC_x$ = 24 m, $ROC_y$ = −16 m; c) Almost perfectly flat STB SESAM.

#260443 Received 3 Mar 2016; revised 13 Apr 2016; accepted 13 Apr 2016; published 4 May 2016
© 2016 OSA

## 4. Thermal lensing: continuous wave (cw) measurements

The thermal lensing of a SESAM originates from different thermally induced effects, such as a temperature dependence of the refractive indices in the various semiconductor layers ($dn/dT$), and bulging or stress due to the thermal expansion of these layers relative to the heat sink [33]. We focus here on a systematic experimental study of our SESAMs in order to determine the implications for high power laser oscillators. A theoretical approach towards understanding these issues is challenging, especially due to the complex heat transfer in the multi-layer structure of a SESAM. Standard simulations are based on finite element method software. They, however, do not capture quantum effects such as phonon reflections, which take place due to the nm-scale of our layer thicknesses, and therefore can hardly provide useful predictions for this purpose.

Therefore, we investigated the thermal properties of our SESAMs using the setup depicted in Fig. 5(a). In a first step, we used a single transverse fundamental mode cw beam at a wavelength of 1030 nm as a localized heat source. Here, for better comparison, we tested only the STND, the FCB, and the STB SESAM, i.e. SESAMs with similar nonlinear behavior but different contacting techniques. This experiment was carried out for SESAM spot size diameters ($1/e^2$) of 800 µm, 400 µm, and 200 µm. We increased the average power up to 300 W while simultaneously tracking the sample temperature using a thermal camera (FLIR SC640) and the sample focal power changes with our interferometer, see Fig. 5(b). For all measurements, we took the cold samples as reference surfaces. The SESAMs' heat sinks were water-cooled to stay at constant room temperature. For calculating the SESAMs' focal powers, we used an evaluation mask sized three times larger than the beam diameter on the sample. Thus, we captured the sample lensing on >99% of the power of our laser beam. With our measurement routine we tracked the most relevant thermal aberrations of our samples, which primarily consist of 2nd order spherical aberrations.

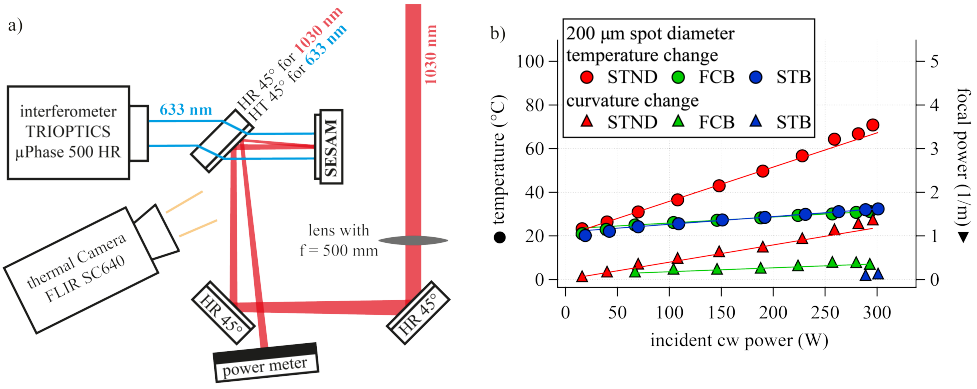


Fig. 5. a) Measurement setup for thermal lensing and temperature rise: a high power single transverse fundamental mode continuous wave or pulsed beam at a center wavelength of 1030 nm is focused onto the SESAM under test. The rise in temperature is tracked by a thermal camera and the change in curvature is recorded by an interferometer. b) Measurement results for continuous wave beams for 200 µm of spot diameter. A clear linear increase in both temperature and focal power is observed. For the slope values extracted from all continuous wave measurements, see Table 1.

Both temperature rise and focal power change showed a linear behavior with the incident pump power, see Fig. 5(b). The resulting slopes of the cw measurements are summarized in Table 1, where the temperature increase $T/P_{inc}$ is indicated in °C/$W_{incident}$, and the focal power change $F/P_{inc}$ in $m^{-1}/kW_{incident}$. It should be noted that all thermal lensing was determined to be non-astigmatic, confirming the isotropic thermal properties of the samples.

#260443 Received 3 Mar 2016; revised 13 Apr 2016; accepted 13 Apr 2016; published 4 May 2016
© 2016 OSA

**Table 1. Summary of continuous wave measurements, showing the temperature and curvature increases per incident continuous wave power unit for different beam spot diameters for the three different bonding techniques. The temperature increase $T/P_{inc}$ is indicated in °C/$W_{incident}$, the focal power increase $F/P_{inc}$ in $m^{-1}/kW_{incident}$.**

| Spot diameter | | STND | FCB | STB |
|---|---|---|---|---|
| 800 µm | $T/P_{inc}$ (°C/$W_{incident}$) | 0.12 | 0.02 | 0.02 |
| | $F/P_{inc}$ ($m^{-1}/kW_{incident}$) | 0.7 | 0.2 | - |
| 400 µm | $T/P_{inc}$ (°C/$W_{incident}$) | 0.13 | 0.03 | 0.03 |
| | $F/P_{inc}$ ($m^{-1}/kW_{incident}$) | 1.5 | 0.5 | - |
| 200 µm | $T/P_{inc}$ (°C/$W_{incident}$) | 0.15 | 0.03 | 0.04 |
| | $F/P_{inc}$ ($m^{-1}/kW_{incident}$) | 4 | 0.9 | - |

At 300 W of incident cw power, we measured (see Fig. 2 for the sample definition):

- STND samples: We measured absolute temperature rises of 36°C, 39°C, and 45°C for decreasing spot size on the sample (resp. 800 m, 400 um, 200 um) and a strong resulting thermal lensing (ROCs of 10 m, 5 m, 2 m) compared to the cold sample.
- FCB samples: As expected, we observed significantly better heat removal compared to STND samples. We measured temperature rises of 6°C, 8°C, and 9°C respectively. Furthermore, the resulting focal power change (ROCs of 35 m, 15 m, 8 m) due to the thermal load of FCB samples was significantly reduced compared to STND samples.
- STB samples: These SESAMs showed the same improvement in temperature rise as our FCB samples. Additionally, they stayed almost perfectly flat up to the maximum incident power of 300 W, with only negligible thermal lensing measurable at the highest power levels. This difference in curvature change of the STB SESAMs compared to the FCB samples most likely originates in the µm thick metal soldering layer between the SESAM structure and the heat sink for FCB samples. It mostly consists of indium (Young's modulus of 11 GPa). On the contrary, for STB SESAMs the epitaxial layers are directly and rigidly bonded onto a stiff SiC heat sink which strongly reduces any type of deformation.

## 5. Thermal lensing: pulsed measurements and comparison of samples at different loss levels

### *5.1 Pulsed measurements*

We repeated the measurements described in the previous section with a high-energy SESAM-modelocked thin disk laser (2.4 MHz repetition rate, up to 60 W of average power, i.e. 25 µJ of pulse energy, at 860 fs pulse duration and 1030 nm center wavelength). It should be noted that we did not carry out systematic pulsed measurements with the smallest spot size diameter of 200 µm, as our SESAMs would be driven deeply in the rollover regime, leading to SESAM damage in accordance to our findings [20]. This damage threshold is inherently linked to the SESAM's nonlinear behavior, more specifically to the extra absorption due to the rollover. It therefore remains unaltered by the contacting technique, as long as the maximum temperature rise stays below potential damage levels of the corresponding mounting process. For the STND and FCB bonding techniques, this corresponds to ≈150°C, and for STB bonding it is >200°C, which is not reached in our experiment.

Exemplary measurements for 400 µm diameter spot size on the STND SESAM are shown in Fig. 6. In contrast to cw operation, where the SESAM is operated at a constant loss level, in pulsed operation the loss saturates with incident power, see Fig. 6(a). Furthermore, additional losses due to the rollover occurring at very large fluence also influence the temperature rise and thermal deformation. This is particularly important for the case of thin disk lasers, which can operate at very strong saturation levels, close to and even beyond this rollover point. For

#260443 Received 3 Mar 2016; revised 13 Apr 2016; accepted 13 Apr 2016; published 4 May 2016
© 2016 OSA

different SESAM saturation levels (such as for 0.8% loss (red) and 1.3% loss (blue) taken as example data points in our measurements) we obtain different absorbed powers by the SESAM and therefore the increase in temperature and focal power is nonlinear, see Fig. 6(b). In order to evaluate our data, we approximated our losses to increase exponentially, which is in good agreement with the SESAM's nonlinear behavior in this fluence regime, see Fig. 6(a). From the exponential fits to our temperature and focal power curves we extract two slopes, corresponding to the values for 0.8% (red) and 1.3% (blue) SESAM losses, respectively, see Fig. 6(b).

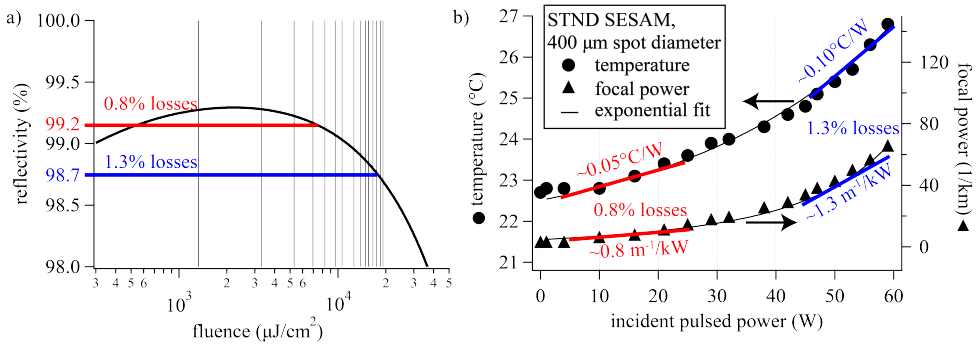


Fig. 6. Measurement for 400 μm spot diameter on the STND samples with average powers reaching up to 60 W (2.4 MHz pulse repetition rate, 1 ps pulse duration, 1030 nm center wavelength). a) Fit extracted from nonlinear reflectivity measurement of our STND SESAM, see Fig. 3(b), with each vertical line indicating one measurement point. b) Temperature and focal power increase over the whole pulsed measurement range. The black solid curve represents an exponential fit to our data. For pulsed incident powers corresponding to roughly 0.8% and 1.3% SESAM loss (indicated by the red and blue line in a) we extracted the slopes to our exponential fit. The corresponding temperature and focal power rises are 0.05°C/$W_{incident}$, 0.8 $m^{-1}$/$kW_{incident}$ (0.8% SESAM losses), and 0.10°C/$W_{incident}$, 1.3 $m^{-1}$/$kW_{incident}$ (1.3% SESAM losses).

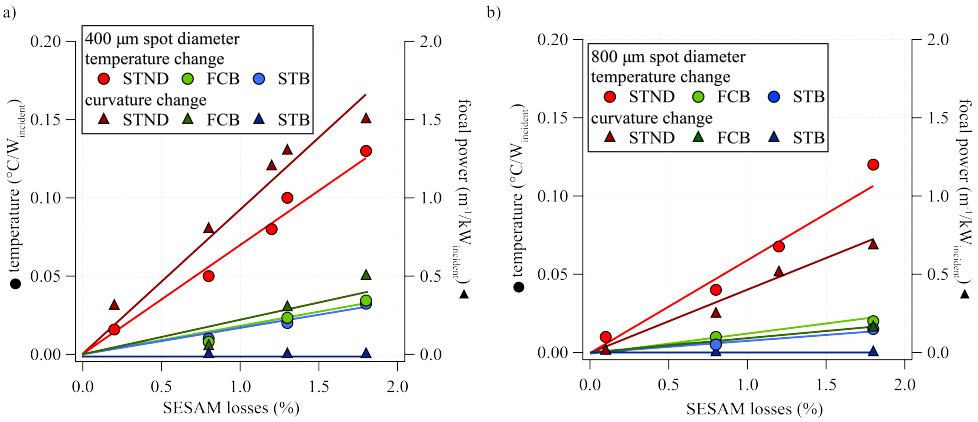


Fig. 7. Combined data from both our continuous wave and pulsed measurements: temperature changes (in °C/$W_{incident}$) and focal power changes (in $m^{-1}$/$kW_{incident}$) for 400 μm (a) and 800 μm (b) spot diameters. A clear linear dependence with the SESAM losses (i.e. with the absorbed average power) is visible, see also Table 2.

In Fig. 7, we combine all data extracted from our cw and pulsed measurements in different SESAM saturation regimes (both before and after the rollover point). We plot the obtained temperature increase slopes and focal power changes against the corresponding SESAM losses. For these plots, we added measurements carried out on our low-loss STND

#260443 Received 3 Mar 2016; revised 13 Apr 2016; accepted 13 Apr 2016; published 4 May 2016
© 2016 OSA

SESAM to the measurements on our STND SESAMs. This allows us to investigate the influence of different nonsaturable loss levels on the SESAM thermal properties. The slopes of the curves presented in Fig. 7, i.e. the resulting values for temperature change per absorbed power, $T/P_{abs}$ in °C/$W_{absorbed}$, as well as focal power change per absorbed power, $F/P_{abs}$ in $m^{-1}/kW_{absorbed}$, are summarized in Table 2. Additionally to our measurements for 800 µm and 400 µm of spot diameter, we include the values for 200 µm of spot diameter (measured only in cw operation). For this, we assumed the same linear dependence on the absorbed power as shown in the 400 µm and 800 µm beam spot diameter cases.

**Table 2. Summary of all continuous wave and pulsed measurements, showing the temperature and curvature increases per absorbed power unit for different beam spot diameters for the three different bonding techniques. The temperature increase $T/P_{abs}$ is indicated in °C/$W_{absorbed}$, the focal power increase $F/P_{abs}$ in $m^{-1}/kW_{absorbed}$.**

| Spot diameter | | STND | FCB | STB |
|---|---|---|---|---|
| 800 µm | $T/P_{abs}$ (°C/$W_{absorbed}$) | 6.6 | 1.1 | 1.1 |
| | $F/P_{abs}$ ($m^{-1}/kW_{absorbed}$) | 40 | 10 | - |
| 400 µm | $T/P_{abs}$ (°C/$W_{absorbed}$) | 7.2 | 1.6 | 1.6 |
| | $F/P_{abs}$ ($m^{-1}/kW_{absorbed}$) | 83 | 28 | - |
| 200 µm (inferred from cw measurement) | $T/P_{abs}$ (°C/$W_{absorbed}$) | 8.4 | 2.2 | 2.2 |
| | $F/P_{abs}$ ($m^{-1}/kW_{absorbed}$) | 220 | 50 | - |

From these measurements, we can conclude the following points with respect to thermal effects in optically loaded SESAMs (see Fig. 2 for the sample definition):

- The temperature increase of both substrate-removed samples (FCB and STB SESAMs) is, as expected, significantly lower than the one of STND SESAMs for the same optical load and loss level. This is beneficial for reduced thermal lensing at high power levels, as well as to avoid undesired variations of the SESAM parameters due to strong temperature gradients [34].
- Both substrate removed SESAMs (FCB and STB) show significantly reduced thermal lensing compared to STND SESAMs. The STB sample shows the smallest lensing of all samples: we were not able to measure a focal power change within the accuracy of our setup both in cw and pulsed operation.
- For all samples the measured temperature increase (in °C/W) as well as focal power increase (in $m^{-1}/kW$) depend linearly on the absorbed power. The absorbed power is set by the saturation level of the SESAM (saturable and nonsaturable losses). This implies that low-loss and strongly saturated SESAMs are beneficial in order to experience the lowest temperature rise and thermal lensing in modelocked operation. However, operation close to the rollover can lead to modelocking instabilities and damage, therefore a trade-off needs to be found for a certain laser system.

*5.2 Implications for kilowatt-class thin disk lasers*

The measured thermal lensing can be used to estimate the behavior of these SESAMs in future kilowatt-class thin disk lasers (TDLs). In order to do this, extrapolating the measured thermal lensing data (performed at small spot sizes of maximum 800 µm) to larger spot sizes (>1 mm) is necessary. The precise scaling behavior of these focal power changes with spot size is difficult to evaluate precisely as it depends on a number of different effects in our multi-layer semiconductor structure. However, our data indicate that a power law scaling proportionality can be assumed, in a similar way to [35]. Therefore, as a conservative upper limit approach, we assume a $1/x$ dependence of thermal lensing with spot size. As we mentioned in the introduction, a realistic estimation for the absorbed power in a low-loss SESAM used in kilowatt-class TDLs is in the order of few tens of watts. Thus, we use 10 W

#260443 Received 3 Mar 2016; revised 13 Apr 2016; accepted 13 Apr 2016; published 4 May 2016
© 2016 OSA

of absorbed power as a reference value for the following example. With this approximation we estimate that:

- On STND SESAMs the resulting estimated focal power change at 10 W of absorbed power will be
  - <0.15 $m^{-1}$ for 2.5 mm laser spot diameter
  - <0.07 $m^{-1}$ for 5 mm spot diameter.
- For FCB SESAMs we estimate focal power changes of
  - <0.05 $m^{-1}$ at 2.5 mm spot diameter and
  - <0.02 $m^{-1}$ at 5 mm spot diameter.
- For STB SESAMs the surfaces will most likely stay practically flat for all spot sizes and absorbed power levels.

If we compare these results to the cavity stability zones depicted in Fig. 1, we can conclude that the deformation due to thermal lensing is currently not the major limiting factor with respect to cavity stability when scaling the spot size in future kilowatt-class TDLs. A more crucial aspect is the optimization of mounting to reach a good cold surface quality, as mentioned in Section 3.

However, in this particular example presented above, we used a SESAM with extremely low losses (<0.1% nonsaturable loss). This is justified for TDLs such as the one in [6, 7], where pulse durations are in the order of several hundred femtoseconds to picoseconds. However, current trends in the development of high power TDLs are pushing toward reaching shorter pulses at these high power levels [8, 28]. The SESAMs for these future systems will most likely have slightly higher nonsaturable loss, thus thermal lensing will be increased accordingly and could potentially reach critical levels. In addition, when considering other modelocked laser systems such as fiber lasers, SESAMs with much higher modulation depth are required to achieve modelocking. In this case, the loss level at a given saturation can be significantly higher. This results in much higher absorbed powers and therefore in much stronger temperature rises and thermal lensing than the ones discussed in our example case here.

## 6. Outlook and conclusion

In this study, we thoroughly investigated the surface quality and thermal properties of high-damage threshold SESAMs designed for future spot size scaling of modelocked thin disk lasers to the kilowatt average power regime. In particular, we studied different substrate-removal and bonding techniques (standard soldering, vacuum soldering, direct bonding) which can be applied to large samples, and compared their performance. As a result of our investigation, novel GaAs-substrate removed SESAMs directly bonded on super-polished SiC substrates (STB samples) were developed which outperform current standard SESAMs in terms of surface quality and heat removal. These samples should enable the next steps in average power and pulse energy scaling of high power oscillators.

Our study shows that (see Fig. 2 for the sample definition):

- The substrate-removal and bonding does not influence the nonlinear parameters of the samples. Only small surface imperfections were observed after processing in the case of the STB samples, which did not affect the losses of the samples for small spot sizes. For large spot sizes (>>5 mm), improved epitaxial material needs to be used, which is an ongoing topic of investigation. All samples used for this study have been designed for high-damage threshold using our guidelines [20] and have

#260443 Received 3 Mar 2016; revised 13 Apr 2016; accepted 13 Apr 2016; published 4 May 2016
© 2016 OSA

ideal parameters for power scaling of modelocked TDLs in different operation regimes.

- The cold surface quality of SESAMs strongly dependents on the contacting technique. Among the techniques compared in this paper, STB samples show orders of magnitude improved cold surface flatness compared to STND or FCB samples, mainly due to the stress-less technique used for the bonding.
- For all samples under test, the rise in temperature and focal power under optical load shows a linear dependence with the power absorbed by the SESAM at its operation point. Substrate-removed samples exhibit an improvement of an order of magnitude in heat removal (temperature rise) and thermal lensing compared to STND samples with the same optical load. In particular, STB SESAMs show only negligible surface deformation.

Our study thus allows us to draw several important conclusions for the future use of these SESAMs in high power TDL operation:

- **Cold surface requirements**: In current state-of-the-art systems, spot size scaling is mainly limited by the cold surface aberrations of the SESAM. To overcome this, special attention needs to be paid to the contacting technique. We quantified this effect for all studied samples and found that STND and FCB SESAMs will need to be improved to avoid resonator instabilities and beam quality degradation in future kilowatt-class TDL oscillators. In contrast, STB SESAMs show perfectly flat cold surfaces and thus fulfill the needed requirements for spot size scaling.
- **Heat removal and thermal lensing**: Another important aspect for future power scaled oscillators consists of minimizing thermally-induced effects such as thermal deformation. Under optical load, substrate-removed samples (FCB and STB) show significantly lower thermal lensing and temperature increases compared to STND samples. Although the levels of thermal lensing measured in this study appear to be small and do not seem to be the main limitation to power scaling of TDLs to the kilowatt-level so far, both a high operating temperature and strong thermal lensing are undesired for long term reliability. Furthermore, other laser systems where faster SESAMs with higher modulation depths are required might be limited by these unwanted thermal effects at much lower average power levels, and substrate removal is therefore critical.

In follow-up efforts, we aim to investigate further possibilities to improve the cold surface aberrations of our STND and FCB samples. This includes using stiffer heat sink materials whose coefficient of thermal expansion is matched to GaAs such as copper diamond DC60, optimizing the pressure distribution in our vacuum soldering setup and investigating alternative gluing options. Furthermore, we will extend the techniques presented here to large-area (>1 $cm^2$) SESAMs. Additionally, we will undertake an in-depth investigation of the surface homogeneity of our samples. In these first experiments, the surface of our STB samples still showed some small imperfections, mainly consisting of small cracks and point-like defects originating from the MBE growth process. These defects may adversely impact the effective nonsaturable losses of the samples when applying very large laser beams and is not visible with the small probe beams used to characterize the reflectivity in the experiments outlined here. Furthermore, involved simulations of the heat dissipation in our various SESAMs will enable optimization of the thermal management of these structures.

To conclude, we are confident that the novel SESAMs presented here will fulfill all the requirements for the next step in power scaling of modelocked thin disk lasers. They will be a

#260443 Received 3 Mar 2016; revised 13 Apr 2016; accepted 13 Apr 2016; published 4 May 2016
© 2016 OSA

crucial cavity component for extending SESAM-modelocked thin disk lasers towards and beyond the kilowatt average power and millijoule pulse energy regime.

**Acknowledgments**

We acknowledge support of the technology and cleanroom facility FIRST of ETH Zurich for advanced micro- and nanotechnology. Additionally, we are thankful for financial support received by the Swiss National Science Foundation (SNSF). Thomas Südmeyer acknowledges support from the European Research Council (ERC) for the project "Efficient megahertz XUV light source" (ERC starting grant 2011 #279545). Crystalline Mirror Solutions acknowledges support from the Austria Wirtschaftsservice (AWS) pre-seed and seed financing program. A portion of this work was performed in the University of California, Santa Barbara Nanofabrication Facility.

#260443 Received 3 Mar 2016; revised 13 Apr 2016; accepted 13 Apr 2016; published 4 May 2016
© 2016 OSA